

Low contrast detectability and spatial resolution with model-based Iterative reconstructions of MDCT images: a phantom and cadaveric study

Domitille Millon¹ · Alain Vlassenbroek² · Aline G. Van Maanen³ · Samantha E. Cambier³ · Emmanuel E. Coche¹

Received: 10 February 2016 / Revised: 22 April 2016 / Accepted: 23 May 2016 / Published online: 14 June 2016
© European Society of Radiology 2016

Abstract

Objectives To compare image quality [low contrast (LC) detectability, noise, contrast-to-noise (CNR) and spatial resolution (SR)] of MDCT images reconstructed with an iterative reconstruction (IR) algorithm and a filtered back projection (FBP) algorithm.

Methods The experimental study was performed on a 256-slice MDCT. LC detectability, noise, CNR and SR were measured on a Catphan phantom scanned with decreasing doses (48.8 down to 0.7 mGy) and parameters typical of a chest CT examination. Images were reconstructed with FBP and a model-based IR algorithm. Additionally, human chest cadavers were scanned and reconstructed using the same technical parameters. Images were analyzed to illustrate the phantom results.

Results LC detectability and noise were statistically significantly different between the techniques, supporting model-based IR algorithm ($p < 0.0001$). At low doses, the noise in FBP images only enabled SR measurements of high contrast objects. The superior CNR of model-based IR algorithm enabled lower dose measurements, which showed that SR was dose and contrast dependent. Cadaver images reconstructed with model-based IR illustrated that visibility and delineation

of anatomical structure edges could be deteriorated at low doses.

Conclusion Model-based IR improved LC detectability and enabled dose reduction. At low dose, SR became dose and contrast dependent.

Key Points

- Model-based Iterative Reconstruction improves detectability of low contrast object.
- With model-based Iterative Reconstruction, spatial resolution is dose and contrast dependent.
- Model-based Iterative Reconstruction algorithms enable improved IQ combined with dose-reduction possibilities.
- Improvement of SR and LC detectability on the same IMR data set would reduce reconstructions.

Keywords Multi Detector CT · Model-Based Iterative Reconstruction · Dose and Image Quality · Phantom · Human cadavers

Introduction

For decades, Filtered Back Projection (FBP) has been the standard as a CT analytical image reconstruction technique [1]. While it is a very fast and robust method, FBP is a sub-optimal algorithmic choice for poorly sampled data or for cases where noise overwhelms the image signal. More recently, iterative reconstruction (IR) techniques were explored that attempt to formulate image reconstruction as an optimization problem. IR techniques require the introduction of a model for the noise estimation and the noisiest measurements are given low weight in the iterative process. Therefore, they contribute very little to the final image and, consequently, reduce the noise present in the reconstructed images.

✉ Domitille Millon
domitille.millon@uclouvain.be

¹ Department of Radiology and Medical Imaging, Cliniques Universitaires Saint Luc, Université Catholique de Louvain, Avenue Hippocrate 10, 1200 Brussels, Belgium

² Philips Healthcare, Rue des deux gares 80, 1070 Brussels, Belgium

³ Statistics Unit, King Albert II Cancer Institute, Université Catholique de Louvain, Avenue Hippocrate 10, 1200 Brussels, Belgium

This results in an overall improvement of image quality (IQ) at any given dose. Two mathematically different iterative approaches were successively introduced. Hybrid algorithms were introduced first, combining analytical and iterative methods in different combinations. This approach used a statistical iterative optimization, based on photon statistics, assuming an ideal system. More recently, model-based approaches based on fully IR emerged, which in addition to hybrid algorithms, attempted to model the system and acquisition process, including the real system optics [2–4].

IQ in CT can be described using several parameters such as image noise, low-contrast detectability (LC), contrast-to-noise ratio (CNR) and spatial resolution (SR). In FBP images, all these parameters are interconnected and the relationships between them are known [5]. At a given dose, an increase in SR generates an increase in noise leading to a reduction of LC objects detectability due to a decreased CNR. Increasing the patient dose is then the only alternative to maintain the LC detectability.

With the introduction of IR, the noise penalty is largely reduced, and these new techniques pave the way to low-dose imaging with improved LC detectability and SR. The purpose of this work was to compare the IQ (LC detectability, noise, CNR and SR) of structures of various sizes and contrast in multi-detector computed tomography (MDCT) images reconstructed with a model-based IR algorithm and with a FBP algorithm at various dose levels.

Materials and methods

The experimental study was performed on a 256-slice MDCT (Philips-HealthCare, Cleveland, OH). A Catphan 500 phantom (The-Phantom-Laboratory, Salem, NY) containing a CTP486 module (Image Uniformity), a CTP515 module (Low Contrast: LC) and a CTP401 module (CT# linearity) (Fig. 1a) was imaged at 120 kilo-Voltage-peak (kVp) and tube-current values ranging from 10 mAs to 720 mAs (8 dose levels) corresponding to Size-Specific Dose Estimates (SSDE) [6, 7] of 1.2 to 85.8 mGy, respectively, for an average phantom Effective Diameter (ED) of 20.3 cm. The acquisition parameters are given in Table 1.

Images were reconstructed with slice thicknesses of 1 mm and 3 mm, using a Field-of-View (FOV) of 250 mm and a matrix 768^2 , both with FBP and a model-based IR technique (IMR-Prototype, Philips-Healthcare, Cleveland, OH) [3]. YA Filters with an Edge Enhancement of -0.75 and YB filters were used for FBP reconstructed images for mediastinum and lung parenchyma, respectively.

Level I (L1) Body Routine and SharpPlus filters were used for IMR reconstructed images for mediastinum and lung parenchyma, respectively. The parameters used for the reconstructed images of each scan were those typically used in chest

CT examinations: the 3-mm-thick-“soft-tissue” images being optimal to visualize the mediastinum in the axial plane and the 1-mm-thin-“lung” axial images being optimal to generate high quality reformatted images of the lung parenchyma, in any plane. The 3-mm-thick-“lung” axial images, although not used in clinical practice, were reconstructed for the purpose of comparison with the 3-mm-thick-“soft-tissue” images.

LC object detection

Four independent observers (DM, EC, ED, AV: 2 radiologists, 1 radiology technician and 1 physicist) counted the number of supra-slice LC objects visible on a slice positioned in the middle of the CTP515 module on each dataset in the axial 1-mm-thin and 3-mm-thick “soft-tissue” and “lung” resolution images. This was counted separately for the three groups of nine objects at 1.0, 0.5 and 0.3 % contrast, respectively, and the results summed to obtain the total number of low-contrast objects visible for each setting. Readers were aware of the number and positions of the objects. One of the four readers (DM) read the images twice to evaluate the intra-reader concordance. Similar luminance conditions (20 lux) were reproduced in the reading room. The images were presented to the observers in a random way. The visualization of each object was graded on a three-level scale by each observer: grade 1.0 - visible as a perfect circle; grade 0.5 - not clearly visible, and grade 0 - not visible. A LC score was calculated by adding the grade values attributed to the detected objects at each of the three contrast levels and converting the sum to a percentage as LC Score = percentage of visible supra-slice objects = $100 * (\#sum-of-grades / 27)$, where 27 was the total number of supra-slice objects. The LC Score could vary from 0 to 100 %. The maximum dose of 48.8 mGy was used to provide a LC Score above 60 % with the 1-mm-thin “lung” resolution axial images for at least one of the reconstruction methods.

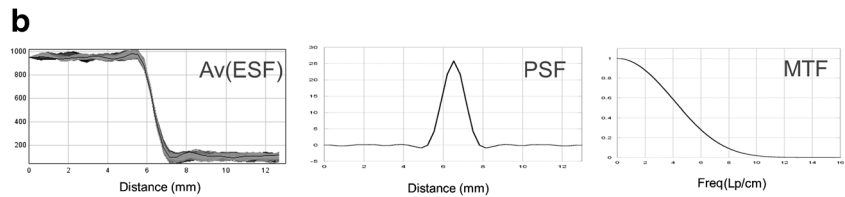
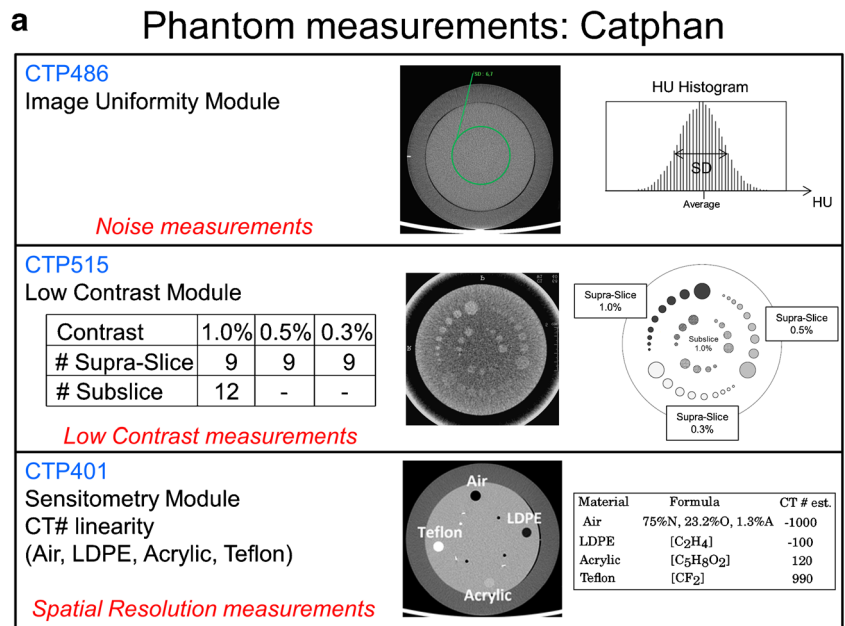
Noise

Measurements were performed on the same datasets. The standard deviation of the Hounsfield Units (HU) was measured in a circular region of interest of 80 mm of diameter placed in the centre of the CTP486 module (Fig. 1a). These measurements were performed at our clinical workstation (EBW v.4.5, Philips Healthcare) with standard tools.

Contrast-to-noise

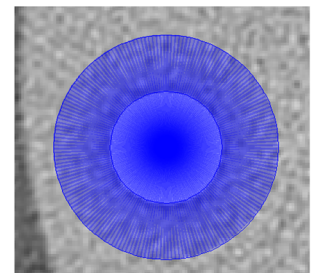
The number of LC objects was also counted separately for the three groups of supra-slice objects at 1.0, 0.5 and 0.3 % contrast, respectively, by each observer. This was performed at each dose level and for the 1-mm-thin and 3-mm-thick “soft-tissue” and “lung” resolution images. The percentage of

Fig. 1 (a) CTP486 module (Image Uniformity), CTP515 module (Low Contrast: LC) and CTP401 module (CT # linearity) of the Catphan phantom used in this study. (b) Modulation Transfer measurements were performed with the edge method applied to the sensitometry inserts of the CTP401 module. The 360 radial profiles separated by 1° were averaged and the average differentiated to obtain the PSF. A Fast Fourier Transform of the PSF was then calculated to obtain the MTF



Edge method applied to sensitometry inserts

- ✓ Av ESF over 360 radial profiles
 increment between profiles = 1°
- ✓ Differentiation of Av(ESF) → PSF
- ✓ MTF = Fast Fourier Transform (PSF)



visible supra-slice objects at each contrast level was calculated as $as = 100 * (\#sum-of-grades) / 9$, where 9 was the total number of supra-slice objects for each contrast level. The corresponding CNR was evaluated by the dividing the corresponding contrast expressed in Hounsfield Units (HU) (10HU, 5HU, 3HU at 1.0, 0.5 and 0.3 % contrast, respectively) by the noise

measured on the CTP 486 module at the same dose and with the same reconstruction settings.

Spatial resolution

Modulation transfer functions (MTF) were measured from the edges of the sensitometry samples of the CTP401 module (Fig. 1a). The edges of each contrast insert were analyzed on the 1-mm-thin “soft-tissue” and “lung” images to determine the average Edge-Spread-Function (average(ESF)) over 360 radial profiles separated by 1°. The central position of each insert was determined from the highest dose images in “soft-tissue” and “lung” resolutions and the same central position was then used for all subsequent measurements performed at lower dose levels. The average(ESF) was differentiated to obtain the Point-Spread-Function (PSF) and Fast-Fourier-

Table 1 Catphan Scans Acquisition Parameters

Collimation (mm)	80
Pitch	0.92
Rotation time (sec)	0.75
kVp	120
mAs	10-720
Body CT DIvol (mGy)	0.7-48.8
Scan length (mm)	255
Dose Length Product (mGy.cm)	21-1464

Transformed (FFT) to obtain the object-specific-MTF (Fig. 1b) [8–10]. An apodization of the PSF using a Gaussian window and a zero-filling to 4096 points was performed before the FFT to avoid spectral leakage [11]. Data analysis was done with a home-made macro built with Image-J software (v.1.49i, National Institute of Health, US) and FFT was performed with Kaleidagraph (v.4.5.0, Synergy-Software, US).

Statistical analysis

Tests to compare the LC scores given a slice thickness using either FBP or IR technique were performed. Parametric assumptions (normal distribution of the data) were first verified. If the normality was not confirmed, a non-parametric test was used for the comparison between the two methods (Wilcoxon test). Three comparative analyses were made: 1) Global: 1-mm-thin “lung” resolution and 3-mm-thick “soft-tissue” resolution at all doses (N=60 measures); 2) 1-mm-thin “lung” resolution at all doses (N=28); and 3) 3-mm-thick “soft-tissue” resolution at all doses (N=32).

Anatomical illustrations

The use of human cadavers fulfilled the requirements of our institutional ethics committee. Chest images of four adult human cadavers (42, 58, 74 and 87 kg average ED=22, 25, 27 and 30 cm respectively) acquired using spiral scans at 80 kVp-10 mAs (body-CTDI_{Vol}=0.2 mGy) and 120 kVp-10, 45, 90 mAs (body-CTDI_{Vol}=0.7, 3.0 and 6.0 mGy, respectively) were reconstructed with parameters identical to the phantom reconstructions but with a FOV=350 mm. The maximum dose of 6.0 mGy was the one used in chest CT examinations for an average size patient at the time FBP was used at our institution. Cadavers were lying down, in decubitus position, with arms up. Lungs were insufflated at total lung capacity. Visibility of anatomical structures between the two reconstruction techniques were analyzed to illustrate the phantom

Table 2 Comparison Between FBP and IMR Techniques

	Low Contrast Scores			
	FBP		IMR	
	1-mm-« lung » resolution	3-mm-« soft-tissue » resolution	1-mm-« lung » resolution	3-mm-« soft-tissue » resolution
N	36	36	32	36
Mean	1.04	5.17	7.91	10.81
Median	0.00	2.75	7.25	11.00
(Min-Max)	(0–12)	(0–17.5)	(0–19)	(0–22)
Missing	0	0	4	0

Table 3 Wilcoxon Test: Comparison Between Techniques

	IMR vs. FBP overall	IMR vs. FBP, 1-mm-« lung » resolution	IMR vs. FBP, 3-mm-« soft-tissue » resolution
V (Variance)	297	62	88
p-value	<0.0001	<0.0001	<0.0001

results. IQ and diagnostic value of the images were assessed by two radiologists (DM and EC).

Results

LC object detection

Normal distribution assumptions were not met for either of the two techniques. The Wilcoxon test showed no significant difference (p=0,40) for intra-reader concordance. Therefore, only the first analysis from this reader was used for the statistical comparisons. The mean and median LC scores are given in Table 2. The global test and the tests according to each slice thickness (1 and 3 mm) showed a significant difference between the two techniques (each p-value <0.0001, Table 3).

Percentage of LC detected objects was statistically significantly different regardless of the slice thickness, supporting the IMR technique (Fig. 2a-b).

Figure 2a-b also shows that, with FBP at a given dose, an increase in SR generates an increase in noise leading to a reduction of LC objects detectability, and that this compromise was much less observed with IMR.

Fig. 2 (a) Comparison between Low Contrast scores obtained with IMR and FBP, averaged between the four readers. Plot of the LC scores as a function of dose: in “soft-tissue” resolution (STD) (red curves) and in “lung” resolution (HR) (blue curves) with 3-mm-thick slices, (b) in “soft-tissue” resolution (red curves) with 3-mm-thick slices and in “lung” resolution (blue curves) with 1-mm-thin slices, (c) comparison between the noise measured with IMR and FBP. Plot of the standard deviation of HU as a function of dose: in “soft-tissue” resolution (red curves) and in “lung” resolution (blue curves) with 3-mm-thick slices, (d) in “soft-tissue” resolution (red curves) with 3-mm-thick slices and in “lung” resolution (blue curves) with 1-mm-thin slices. (e) Plot of the percentage of detected objects as a function of the CNR for all dose levels and all reconstruction techniques. We note a similar fast increase in the percentage of detected objects with FBP (red dots) and IMR (blue dots) when the CNR increases between 0 and 1. With a CNR above 1, the majority of measurements shows a detectability above 70 %. The horizontal arrow shows the improvement in CNR for one particular measurement when going from FBP to IMR (from CNR = 0.23 to CNR = 1.27, respectively), due to the large reduction of noise with IMR. The vertical arrow shows the corresponding increase in detectability (from 36 % to 89 %, respectively)

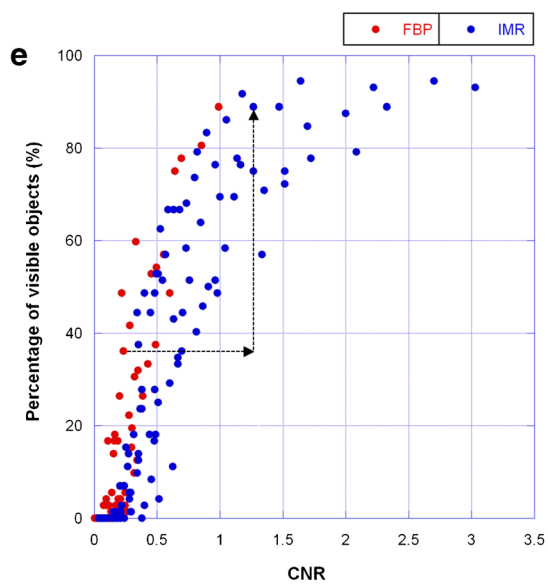
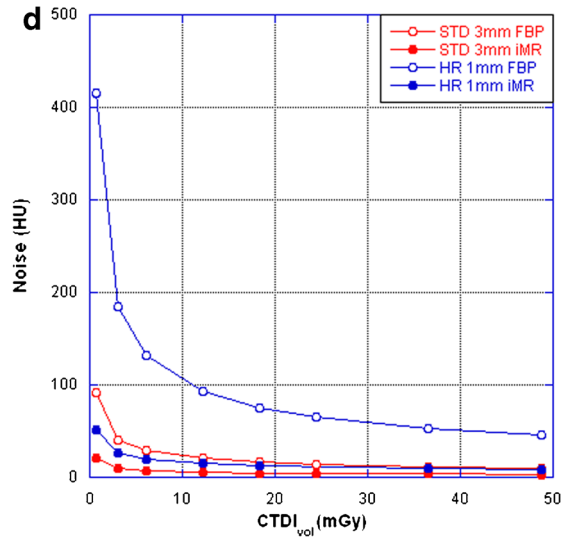
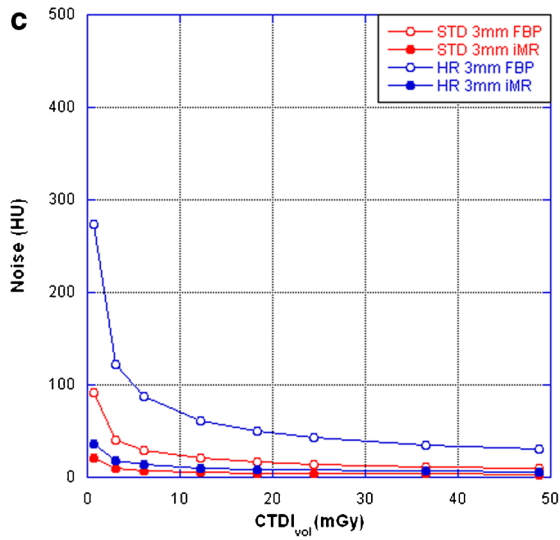
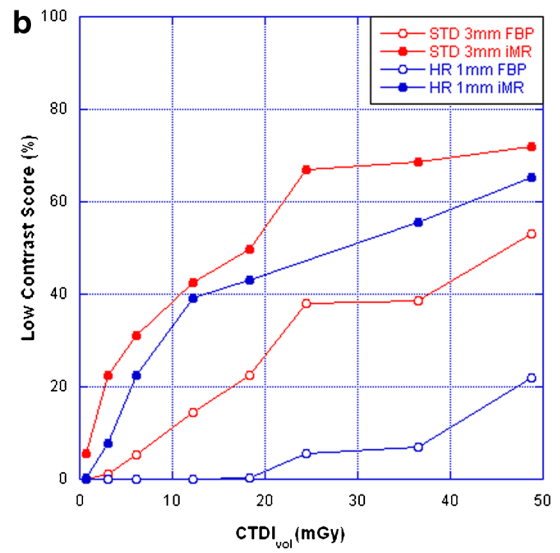
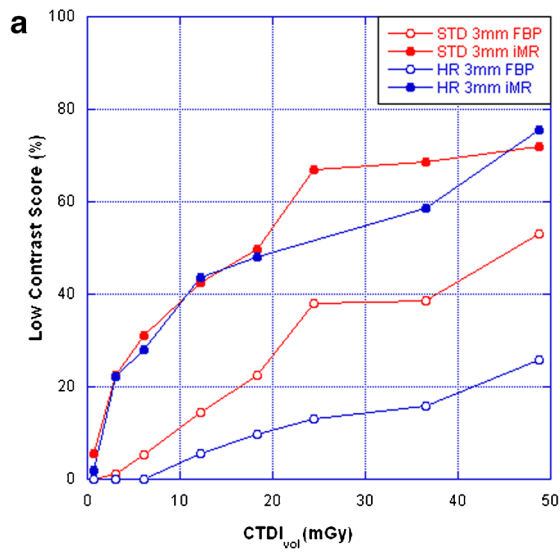


Image noise

IMR provided significant noise reduction compared with FBP. Low noise levels were achieved with IMR even for low dose acquisitions, in “soft-tissue” and “lung” resolutions and with both slice thicknesses (Fig. 2c-d).

Contrast-to-noise

IMR provided major CNR improvements compared with FBP, leading to an increased percentage of detected objects at each contrast level for all dose levels and all reconstruction settings (Fig. 2e).

Spatial resolution

On the CTP401 module, we measured Air = -998 HU, Teflon = 958 HU and Low Density Polyethylene (LDPE) = -87 HU. The Plexiglass background was measured at 103 HU and so the contrast differences between the inserts and the background were measured as -1101 HU, 855 HU and -190 HU, respectively. In our study, air and Teflon were considered as high contrast inserts and LDPE as a low-contrast insert.

No measurements were performed on the fourth acrylic sensitometry insert of the Catphan phantom due to the insufficient Contrast-to-Noise Ratio (CNR) in FBP images between the acrylic insert and the background at all doses. The FBP images of the LDPE insert were only analyzed at the highest dose for the same reason. There was not such a limitation with IMR images. The MTF measured on the high-contrast inserts reconstructed with FBP was not affected by the scan dose neither in “soft-tissue” (Fig. 3a) nor in “lung” (Fig. 3b) resolution. With both reconstruction techniques, the SR measured at the highest dose was not affected by the contrast of the insert (see Fig. 3c-d). However, with IMR, SR was affected by the scan dose. Comparative measurements between a high-contrast insert (Teflon, Fig. 3e-f) and the LC insert (LDPE, Fig. 3g-h) showed that the amount of SR drop was dose and contrast dependent and that it was more pronounced in “lung” (Fig. 3h) than in “soft-tissue” (Fig. 3g) resolution. Table 4 shows the MTF@50 % measured on these inserts at the different doses. With IMR images, the loss of SR was more pronounced at the lowest dose for the lowest contrast insert. MTF curves obtained with the LC insert at the lowest dose in “lung” and “soft-tissue” resolutions were identical (see Fig. 3i). As a consequence, there was no improvement in the visibility of LC details when using “lung” instead of “soft-tissue” resolution.

In other words, the spatial resolution loss with IMR behaved like the inverse of the contrast-to-noise ratio in the FBP technique: the lowest the contrast-to-noise, the largest the spatial resolution loss.

Anatomical illustrations

Similar to phantom images, cadaver images reconstructed with IMR showed a lower noise level compared to FBP with a corresponding improvement in LC detectability. A comparative example is shown in Fig. 4a with a 42 kg-cadaver scanned at 120 kVp successively at 90 mAs and 10 mAs. LC areas, which are visible at full dose (6.0 mGy) in “soft-tissue” resolution with 3-mm-thick slices in FBP, can be completely missed with FBP if drastic dose reduction (0.7 mGy) is applied. With IMR, lesions can still be easily detected at this very low dose level. Another example of a low-dose scan is provided in Fig. 4b: FBP images were non-diagnostic due to an excessive amount of noise while the corresponding IMR images could still provide useful clinical information. The identification of two pre-fissural nodules was much easier on the IMR axial images and distinguishing of mosaic attenuation areas on both sides on IMR axial images was impossible on the FBP images. In this example, the effective dose delivered was very close to the one of a conventional chest X-ray (~0.05 mSv) [12].

Figure 5a-c shows comparative IMR reconstructions demonstrating the loss of details with decreasing doses. Loss of details of the bronchial tree was clearly visible with the most aggressive dose reductions of 88 % (0.7 mGy) and 97 % (0.2 mGy) (Fig. 5a).

Axial images showed a loss of small high-contrast details (vessels) and a loss of larger lower contrast details (bronchial elements) with the most aggressive dose reductions (Fig. 5b).

Figure 5c shows at a same very low-dose level, this loss of details depended on the body attenuation and on the noise contained within the original attenuation profiles. It was the largest with the largest cadaver size.

Discussion

At all dose levels applied to the phantom, we showed substantial LC detectability improvements with noise level reduction on IMR images in comparison with FBP images as previously reported in many papers [8, 13–15]. This improved detectability was due to an improved CNR for each object contrast at all dose levels and for all reconstruction settings, due to the noise reduction with IMR. Such improvements will mainly benefit clinical applications where LC detectability is of primary importance [16–20]. The latter was also much less affected by the SR with IMR than with FBP, reducing the trade-off between LC and SR usually encountered with FBP.

At the highest dose level, LC detectability improvements with IMR were not associated with any SR degradation (similar MTF between FBP and IMR): we could still improve SR on IMR images in comparison with FBP while maintaining the LC detectability to be superior or equal. The superior LC

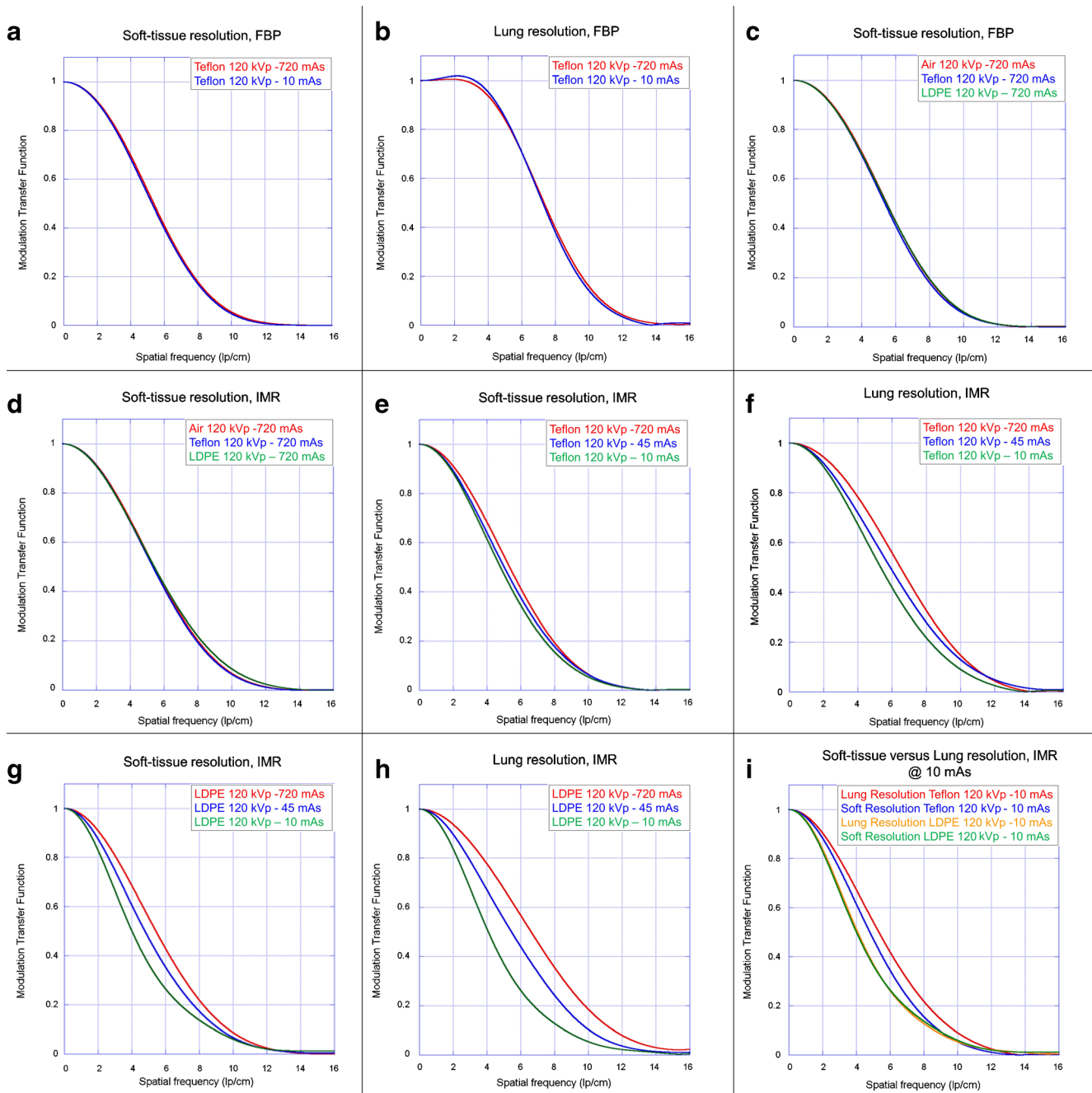


Fig. 3 (a) Results of MTF measurements on: Teflon insert @720 mAs (red) and 10 mAs (blue) in “soft-tissue” resolution (FBP), (b) Teflon insert @720 mAs (red) and 10 mAs (blue) in “lung” resolution (FBP), (c) Air (red)-Teflon (blue) and LDPE (green) inserts @720 mAs in “soft-tissue” resolution (FBP), (d) Air (red)-Teflon (blue) and LDPE (green) inserts @720 mAs in “soft-tissue” resolution (IMR), (e) Teflon insert @720 mAs (red), 45 mAs (blue) and 10 mAs (green) in “soft-

tissue” resolution (IMR), (f) Teflon insert @720 mAs (red), 45 mAs (blue) and 10 mAs (green) in “lung” resolution (IMR), (g) LDPE insert @720 mAs (red), 45 mAs (blue) and 10 mAs (green) in “soft-tissue” resolution (IMR), (h) LDPE insert @720 mAs (red), 45 mAs (blue) and 10 mAs (green) in “lung” resolution (IMR), (i) Teflon insert in “lung” resolution (red) and “soft-tissue” (blue) and LDPE insert in “lung” resolution (yellow) and “soft-tissue” (green) @10 mAs (IMR)

score obtained with 1-mm-thin slices in “lung” resolution with IMR in comparison to the one obtained with 3-mm-thick in “soft-tissue” resolution with FBP, showed the combined improvement of both SR and LC detectability on

the same reconstructed IMR dataset. This approach could significantly simplify the workflow by requiring only one single reconstruction to optimally visualize any organ (e.g., soft tissue, lung, bone) with very high quality. A unique

Table 4 MTF 50 % @120 kVp in LinePairs/cm (lp/cm)

	720 mAs		45 mAs		10 mAs	
	FBP	IMR	FBP	IMR	FBP	IMR
Teflon « soft-tissue »	5.4	5.4	5.4	5.0	5.3	4.8
LDPE « soft-tissue »	5.4	5.4	NA	4.8	NA	4.0
Teflon « lung »	7.3	6.5	7.3	5.9	7.2	5.3
LDPE « lung »	7.3	6.6	NA	5.5	NA	4.1

reconstructed dataset (1-mm-thick “lung”) could be sufficient to explore the entire body. This would require further comparative studies between the two techniques for different applications, but could potentially bring advantages in terms of workflow, image processing time and data storage. This will be the subject of a separate paper.

After 50 % dose reduction, LC detectability was still superior on IMR images compared to the one of FBP images reconstructed from the full 100 % dose scan, all other parameters being identical. The comparison between the 1-mm-thin

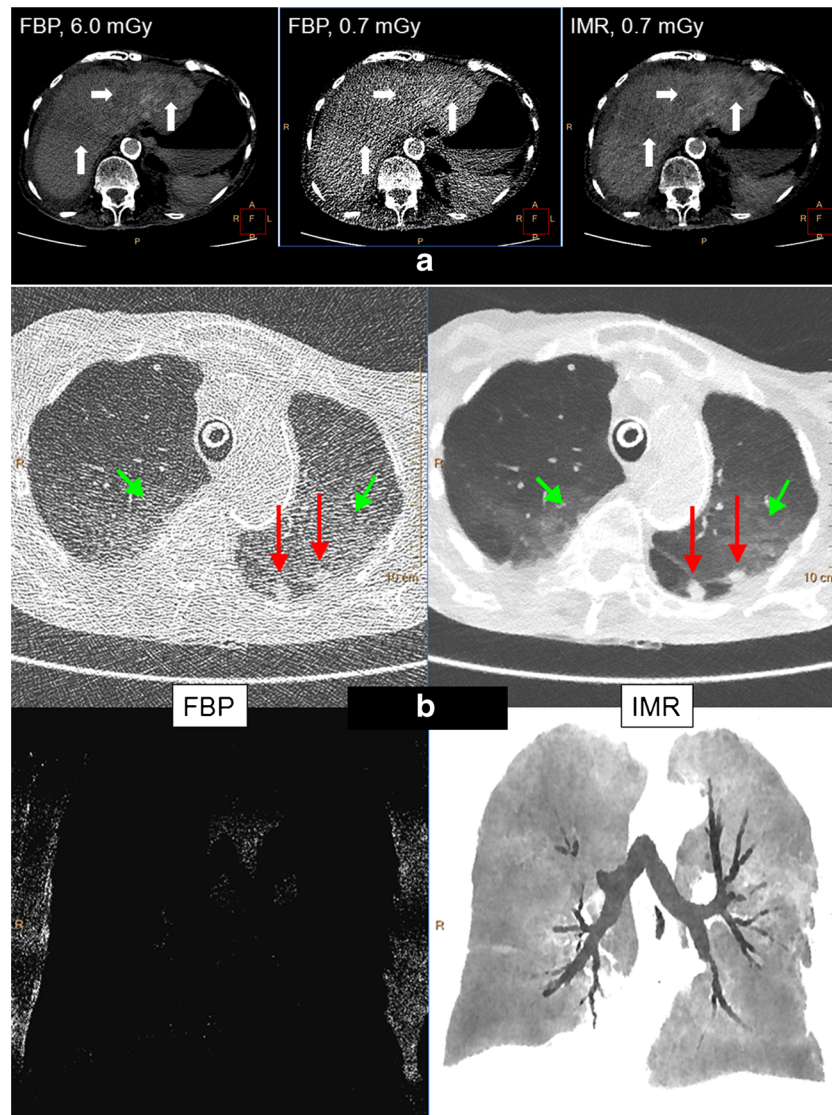
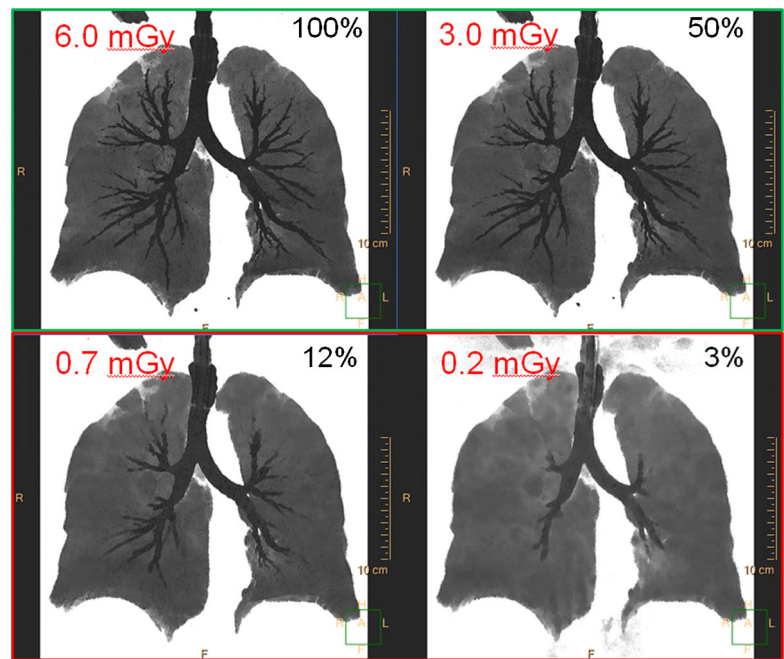


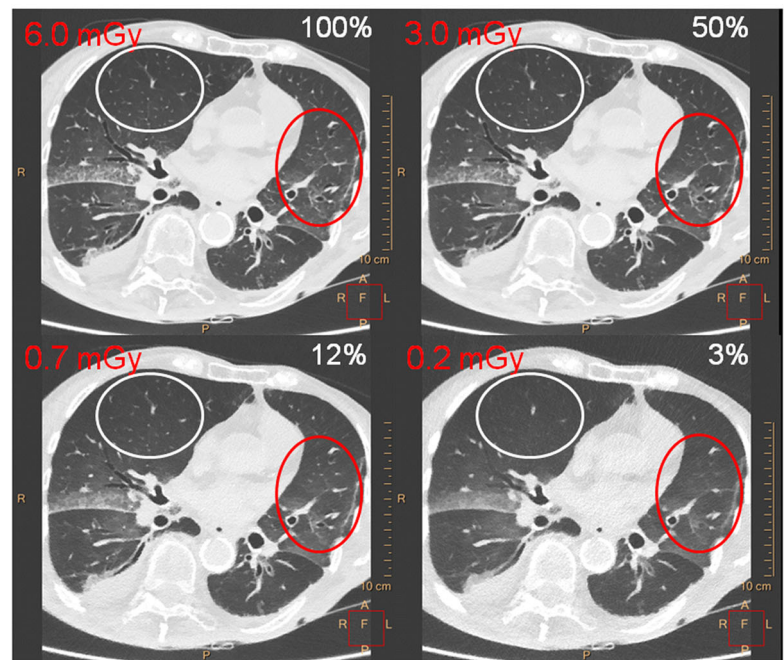
Fig. 4 (a) Comparative axial images illustrating the difference in image quality between FBP and IMR images of a 42 kg human cadaver in the liver ($CTDI_{vol} = 0.7$ mGy). The FBP image at standard dose ($CTDI_{vol} = 6.0$ mGy) is shown for the comparison. The low-contrast regions, which are visible on the 6.0 mGy dose images (white arrows), are still perfectly visible with IMR at 0.7 mGy. These areas are completely masked by the noise on the corresponding FBP images. (b) Axial 1-mm-thin images (upper row) and MinIP of a 20-mm-thick coronal slab (lower row) illustrating the difference in image quality between FBP and IMR

chest images of a 42 kg human cadaver ($CTDI_{vol} = 0.2$ mGy, Eff. Dose = 0.09 mSv). FBP images were non-diagnostic due to an excessive amount of noise, while the corresponding IMR images could still provide useful clinical information. The identification of two prefissural nodules were much easier on the IMR axial images (red arrows) and distinction between mosaic attenuation areas on both sides on IMR axial images (short green arrows) was impossible on the FBP images. Note the difference of visibility of the thorax using the same display settings on these coronal MinIP images

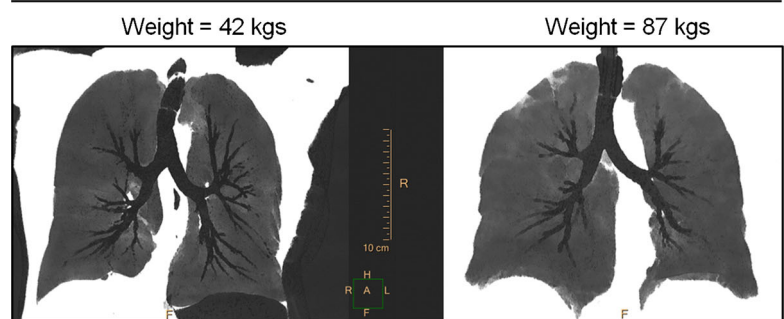
Fig. 5 (a) IMR images of a 87 kg cadaver with decreasing doses. MinIP coronal slabs of thickness = 50 mm: loss of details of the bronchial tree is clearly visible with the most aggressive dose reductions of 88 % (0.7 mGy) and 97 % (0.2 mGy). (b) Comparative 1-mm-thin “lung” resolution axial images. The axial images showed a loss of small high contrast details (white ellipse) and a loss of larger lower contrast details (red ellipse) with the most aggressive dose reductions. (c) IMR images MinIP coronal slabs of thickness = 50 mm of two different cadavers (42 kg and 87 kg) scanned with a $CTDI_{vol} = 0.7$ mGy: loss of details of the bronchial tree depended on the body attenuation and on the noise; this was the largest for the largest cadaver size



a



b



c

“lung” resolution IMR images obtained at 50 % of the dose and the 3-mm-thick “soft-tissue” resolution FBP images obtained at full dose showed similar LC detectability, with an improved SR on IMR images. IQ was improved with IMR with 50 % dose reduction, without consequence for diagnostic performance and further dose reduction could be achieved. Those improvements were confirmed on cadaver images.

Around 80 % dose reduction, LC scores were still significantly superior with IMR images than FBP. However, our results have shown that they were progressively associated with an increasing loss of structures on IMR images when the dose reduction was increased [18, 21, 22]. We primarily observed a loss of LC details, which was more pronounced in “lung” than in “soft-tissue” resolution. As previously shown by Richard et al., SR in model-based IR was dependent on both dose and contrast in opposition to FBP [10]. We noticed that, at low dose, there was no benefit using “lung” instead of “soft-tissue” resolution to improve the visibility of small LC structures. It is very important to point out that these details were already invisible on the FBP images because of the amount of noise present on those images at low dose. Both phantom and human cadaver acquisitions illustrated those results. The cadaver images illustrated that small anatomical LC structures started to disappear on the chest IMR images when the dose was reduced by more than 80 %. In this regard, images acquired at low doses could be non-diagnostic with both FBP and IMR, when the analysis or detection of small LC structures is needed. However the same IMR images could still be very useful for the detection of higher contrast objects (e.g., small solid nodules) when they would be completely useless if reconstructed with FBP due to the excessive amount of noise. Dose reduction is a major challenge and low dose clinical scan protocols which had been optimized based on the CT noise properties of FBP will need to be re-evaluated with model-based IR using new IQ metrics for every single exploration (anatomical region and diseases).

This paper is the first analyzing LC detectability, SR and noise at various doses from phantom scans, confirmed with anatomical illustrations. We used a strong and objective evaluation method to measure the SR on the images of inserts of various contrast, following a published methodology [10, 23]. Many previous studies evaluating IR algorithms measured SR exclusively on high-contrast inserts [8, 24]. These measurements can only provide the maximum SR, which is obtained at very high contrast-to-noise ratio but do not reflect how SR will be affected when the dose/contrast ratio is reduced.

Our study had several limitations. First, readers should have been blinded to the “real number and positions of lesions”. Second, only one model-based IR algorithm was assessed. However, our findings were similar to those described in other papers evaluating model-based IR from other manufacturers [10, 23], confirming the common behaviour of all algorithms.

Without targeting dose reduction, new IMR reconstruction algorithm enabled major IQ improvements by increasing LC and SR at low noise levels. It removed the trade-off between LC and SR usually encountered with FBP, and improved diagnostic performance and workflow.

Dose reduction could be achieved thanks to these IQ improvements, but with very large dose reduction, diagnostic performance could be compromised and scan protocols will need to be re-evaluated.

Acknowledgments A poster has been presented based on these results at the ECR 2015. The scientific guarantor of this publication is Pr Emmanuel COCHE. The authors of this manuscript declare relationships with the following companies: Alain Vlassenbroek is an employee of Philips Healthcare. The authors state that this work has not received any funding. One of the authors has significant statistical expertise. Institutional Review Board approval was obtained. Written informed consent was waived by the Institutional Review Board. Methodology: experimental, performed at one institution.

References

1. Kak ACS, M. (1988) Principles of Computerized Tomographic Imaging Principles of Computerized Tomographic Imaging. Institute for Electrical and Electronic Engineers, IEEE Press
2. Geyer LL, Schoepf UJ, Meinel FG et al (2015) State of the art: iterative CT reconstruction techniques. *Radiology* 276:339–357
3. Mehta D (2013) Iterative model reconstruction: simultaneously lowered computed tomography radiation dose and improved image quality. *Med Phys Int J* 1:9
4. Brown KZS, Koehler T (2012) Acceleration of ML iterative algorithms for CT by the use of fast start images. *Physics of Medical Imaging*, San Diego
5. Goldman LW (2007) Principles of CT: radiation dose and image quality. *J Nucl Med Technol* 35:213–225, **quiz 226–218**
6. (2011) Size-Specific Dose Estimates (SSDE) in Pediatric and adult body CT examinations. *American Association of Physicists in Medicine*, pp 1–26
7. (2014) Use of water equivalent diameter for Calculating Patient Size and Size-Specific Dose Estimates (SSDE) in CT. *American Association of Physicists in Medicine*, pp 1–23
8. Mieville FA, Gudinchet F, Brunelle F, Bochud FO, Verdun FR (2013) Iterative reconstruction methods in two different MDCT scanners: physical metrics and 4-alternative forced-choice detectability experiments—a phantom approach. *Phys Med* 29:99–110
9. Rossmann K (1969) Point spread-function, line spread-function, and modulation transfer function. *Tools for the study of imaging systems. Radiology* 93:257–272
10. Richard S (2012) Towards task-based assessment of CT performance: system and object MTF across different reconstructions algorithms. *Med Phys* 39
11. Naylor DA, Tahic MK (2007) Apodizing functions for Fourier transform spectroscopy. *J Opt Soc Am A Opt Image Sci Vis* 24: 3644–3648
12. Neroladaki A, Botsikas D, Boudabbous S, Becker CD, Montet X (2013) Computed tomography of the chest with model-based iterative reconstruction using a radiation exposure similar to chest X-ray examination: preliminary observations. *Eur Radiol* 23:360–366
13. Gervaise A, Osemont B, Lecocq S et al (2012) CT image quality improvement using adaptive iterative dose reduction with wide-volume acquisition on 320-detector CT. *Eur Radiol* 22:295–301

14. Saiprasad G, Filliben J, Peskin A et al (2015) Evaluation of low-contrast detectability of iterative reconstruction across multiple institutions, CT scanner manufacturers, and radiation exposure levels. *Radiology*. doi:10.1148/radiol.2015141260:141260
15. Klink T, Obmann V, Heverhagen J, Stork A, Adam G, Begemann P (2014) Reducing CT radiation dose with iterative reconstruction algorithms: the influence of scan and reconstruction parameters on image quality and CTDIvol. *Eur J Radiol* 83:1645–1654
16. Korn A, Fenchel M, Bender B et al (2012) Iterative reconstruction in head CT: image quality of routine and low-dose protocols in comparison with standard filtered back-projection. *AJNR Am J Neuroradiol* 33:218–224
17. Rapalino O, Kamalian S, Kamalian S et al (2012) Cranial CT with adaptive statistical iterative reconstruction: improved image quality with concomitant radiation dose reduction. *AJNR Am J Neuroradiol* 33:609–615
18. Baker ME, Dong F, Primak A et al (2012) Contrast-to-noise ratio and low-contrast object resolution on full- and low-dose MDCT: SAFIRE versus filtered back projection in a low-contrast object phantom and in the liver. *AJR Am J Roentgenol* 199:8–18
19. Kilic K, Erbas G, Guryildirim M, Arac M, Ilgit E, Coskun B (2011) Lowering the dose in head CT using adaptive statistical iterative reconstruction. *AJNR Am J Neuroradiol* 32:1578–1582
20. Pickhardt PJ, Lubner MG, Kim DH et al (2012) Abdominal CT with model-based iterative reconstruction (MBIR): initial results of a prospective trial comparing ultralow-dose with standard-dose imaging. *AJR Am J Roentgenol* 199:1266–1274
21. Schindera ST, Odedra D, Raza SA et al (2013) Iterative reconstruction algorithm for CT: can radiation dose be decreased while low-contrast detectability is preserved? *Radiology* 269:511–518
22. McCollough CH, Yu L, Kofler JM et al (2015) Degradation of CT low-contrast spatial resolution due to the use of iterative reconstruction and reduced dose levels. *Radiology* 276:499–506
23. Li K, Garrett J, Ge Y, Chen GH (2014) Statistical model based iterative reconstruction (MBIR) in clinical CT systems. Part II. Experimental assessment of spatial resolution performance. *Med Phys* 41:071911
24. Love A, Olsson ML, Siemund R, Stalhammar F, Bjorkman-Burtscher IM, Soderberg M (2013) Six iterative reconstruction algorithms in brain CT: a phantom study on image quality at different radiation dose levels. *Br J Radiol* 86:20130388